

# A mapping study of L1174 with $^{13}\text{CO } J = 2 - 1$ and $^{12}\text{CO } J = 3 - 2$ : star formation triggered by a Herbig Ae/Be star

Jing-Hua Yuan<sup>1</sup>, Yuefang Wu<sup>2\*</sup>, Jin Zeng Li<sup>1</sup>, Wentao Yu<sup>2</sup>, and Martin Miller<sup>3</sup>

<sup>1</sup>National Astronomical Observatories, Chinese Academy of Sciences, 20A Datun Road, Chaoyang District, Beijing 100012, China

<sup>2</sup>Department of Astronomy, Peking University, 100871 Beijing, China; ywu@pku.edu.cn

<sup>3</sup>I. Physikalisches Institut, Universität zu Köln, Zùlpicher Str. 77, 50937 Cologne, Germany

Accepted 2012 October 31. Received 2012 October 27; in original form 2012 September 3

## ABSTRACT

We have carried out a comprehensive study of the molecular conditions and star-forming activities in dark cloud L1174 with multi-wavelength data. Mapping observations of L1174 in  $^{13}\text{CO } J = 2 - 1$  and  $^{12}\text{CO } J = 3 - 2$  were performed using the KOSMA 3-meter telescope. Six molecular cores with masses ranging from 5 to 31  $M_{\odot}$  and sizes ranging from 0.17 to 0.39 pc are resolved. Large area ahead of a Herbig Be star, HD 200775, is in expanding and core 1 is with collapse signature. Large line widths of  $^{13}\text{CO } J = 2 - 1$  indicate the ubiquity of turbulent motions in this region. Spectra of  $^{12}\text{CO } J = 3 - 2$  prevalently show conspicuously asymmetric double-peaked profiles. In a large area, red-skewed profiles are detected and suggestive of a scenario of global expansion. There is a large cavity around the Herbig Be star HD 200775, the brightest star in L1174. The gas around the cavity has been severely compressed by the stellar winds from HD 200775. Feedbacks from HD 200775 may have helped form the molecular cores around the cavity. Seventeen 2MASS potential young stellar objects were identified according to their 2MASS colour indices. The spatial distribution of the these 2MASS sources indicates that some of them have a triggered origin. All these suggest that feedbacks from a Herbig Ae/Be star may also have the potential to trigger star forming activities.

**Key words:** ISM: clouds – ISM: molecules – ISM: structure – line: profiles – molecular data – Stars: formation

## 1 INTRODUCTION

L1174 is a molecular cloud located in the constellation of Cepheus with low- to intermediate-mass star forming activities (Kun, Kiss, & Balog 2008). As a portion of the L1167/L1174 complex, L1174 was reported for the first time as a dark nebula by Lynds (1962). Investigations of L1174 have been performed with multi-wavelengths continuum and emission lines observations. The first mapping observations with molecular lines were carried out by Myers, Linke, & Benson (1983) in  $^{13}\text{CO } J = 1 - 0$  and  $\text{C}^{18}\text{O } J = 1 - 0$ . Studies with lines from  $^{12}\text{CO}$  and its isotopic variants have been performed by Myers et al. (1988), Wu, Zhou, & Evans (1992), Butner, Lada, & Loren (1995), Bontemps et al. (1996), Williams et al. (1998), Buckle & Fuller (2002), and Walsh, Myers, & Burton (2004). Wing emissions of  $^{12}\text{CO } J = 1 - 0$  were detected in L1174 and interpreted as evidence of outflow activities by Wu, Zhou, & Evans (1992). With observations in  $\text{NH}_3 (J, K) = (1, 1)$ , Goodman et al. (1993) detected an averaged velocity gradient of  $0.87 \pm 0.32 \text{ km s}^{-1} \text{ pc}^{-1}$  in L1174. This region has been studied with lines from

other molecules with mapping and point observations, e.g., HCN and HNC by Harju (1989) and Turner, Pirogov, & Minh (1997),  $\text{C}_3\text{H}_3$  by Madden et al. (1989), CS by Zhou et al. (1989),  $\text{HC}_3\text{N}$  by Fuller & Myers (1993),  $\text{DCO}^+$  and  $\text{H}^{13}\text{CO}^+$  by Butner, Lada, & Loren (1995) and Williams et al. (1998),  $\text{N}_2\text{H}^+$  and  $\text{C}_3\text{H}_2$  by Benson, Caselli, & Myers (1998), and  $\text{CH}_3\text{OH}$ ,  $\text{c-C}_3\text{H}_2$  by Buckle & Fuller (2002). Efforts to search for water masers in L1174 obtained negative results (Persi, Palagi, & Felli 1994; Furuya et al. 2003; Sunada et al. 2007).

Located in L1174, a well known reflection nebula NGC 7023 has been extensively studied. NGC 7023 is illuminated by a Herbig Be star HD 200775 (Kun, Kiss, & Balog 2008). There are 3 photodissociation regions (PDRs) in NGC 7023 located to the east, south and northwest of the exciting star. During the past decade, chemical and physical conditions of these PDRs have been investigated with observations at wavelengths from mid-infrared to millimeter (An & Sellgren 2003; Sellgren, Uchida, & Werner 2007; Berné et al. 2008; Sellgren et al. 2010; Boersma et al. 2010; Abergel et al. 2010; Joblin et al. 2010; Habart et al. 2011; Rosenberg et al. 2011). Many of these studies were dedicated to spectroscopic observations of PAH emission features in this region. The first confirmedly detected fullerene  $\text{C}_{60}$  in

\* E-mail: ywu@pku.edu.cn

interstellar space was discovered in NGC 7023 (Werner et al. 2004; Sellgren, Uchida, & Werner 2007; Sellgren et al. 2010). With observations using SPIRE and PACS onboard *Herschel*, Abergel et al. (2010) for the first time detected far-infrared/submm filaments in the PDRs of NGC 7023.

HD 200775 is a massive Herbig Be star with a spectral type of B3( $\pm 1$ )e and a total luminosity of  $15,000 L_{\odot}$  (Hernández et al. 2004). The binarity of this source was confirmed by Monnier et al. (2006). Alecian et al. (2008) estimated the masses of the primary and the secondary stars to be 10.7 and 9.3  $M_{\odot}$  respectively, and the age of the primary to be about  $10^5$  yr. At the near vicinity, a biconical cavity has been very likely excavated by an energetic bipolar outflow in an earlier evolutionary stage (Fuente et al. 1998). In a recent work, Okamoto et al. (2009) presented the detection of a flared disk around HD 200775.

The distance to L1174 from the Sun has not been firmly determined. In the literature, several values have been quoted, e.g., 440 pc (Wu, Zhou, & Evans 1992; Goodman et al. 1993; Bontemps et al. 1996),  $429_{-90}^{+159}$  pc (van den Ancker, de Winter, & Tjin A Djie 1998), and 288 pc (Straizys et al. 1992). In this paper, we will follow Wu, Zhou, & Evans (1992) to adopt the distance of 440 pc.

In this paper, we will present a mapping study of L1174 with  $^{13}\text{CO } J = 2 - 1$  and  $^{12}\text{CO } J = 3 - 2$ . The physical conditions and kinematics are profoundly discussed. With combination of millimeter and infrared data, star forming activities in L1174 are well investigated. This paper is arranged as follows: we present a description of the observations and archival data in Section 2, while the results and some preliminary analysis are presented in Section 3; in Section 4, we try to comprehensively discuss the data; the findings of this work are summarized in Section 5.

## 2 OBSERVATIONS AND DATA ACQUISITION

### 2.1 KOSMA observation

A region of  $23' \times 15'$  around L1174 was mapped in  $^{13}\text{CO } J = 2 - 1$  (220.399GHz) and  $^{12}\text{CO } J = 3 - 2$  (345.796GHz) using the Kölner Observatorium für SubMillimeter Astronomie (KOSMA) 3-m telescope<sup>1</sup> on Gornergrat near Zermatt in Switzerland. The observations were carried out with a  $1' \times 1'$  grid using the on-the-fly (OTF) mode on April 16th 2003. The reference point was at ( $\alpha = 21^{\text{h}}00^{\text{m}}22^{\text{s}}.13$ ,  $\delta = 68^{\circ}12'52''.9$ , J2000).

The  $^{13}\text{CO } J = 2 - 1$  and  $^{12}\text{CO } J = 3 - 2$  lines were simultaneously observed with the dual-channel 230/345 GHz SIS receiver (Graf et al. 1998), whose noise temperature was about 120 K. The on board acousto optical spectrometer (Schieder, Tolls, & Winnewisser 1989) had 1501 and 1301 channels with bandwidths of 248 and 442 MHz at 230 and 345 GHz respectively. This resulted in channel widths of 165 and 340 kHz corresponding to velocity resolutions of 0.22 and 0.29  $\text{km s}^{-1}$  at 230 and 345 GHz. The system temperatures,  $T_{\text{sys}}$ , were 186 and 245 K at 230 and 345 GHz. The beam sizes at 230 and 345 GHz were determined to be  $130''$  and  $80''$  with continuum cross scans on Jupiter. The forward efficiency  $F_{\text{eff}}$  was 0.93 during our observations. And the main beam efficiencies  $B_{\text{eff}}$  were 0.68 and 0.72 at 230 and 345 GHz. The pointing was frequently checked on Jupiter and better than  $10''$ .

The data were reduced and visualized with CLASS and GREG programs of GILDAS software (Pety 2005). The baselines were fitted with one order polynomial and removed for each line. The line

intensities were corrected to main beam temperature scale using the formula of  $T_{\text{mb}} = T_{\text{A}}^* F_{\text{eff}} / B_{\text{eff}}$ .

### 2.2 Archival data

The *Spitzer* Gould Belt Legacy Survey<sup>2</sup> (program ID: 30574; Allen & Spitzer Gould Belt Legacy Team 2007) carried out observations toward L1174 and its vicinity with the InfraRed Array Camera (IRAC; Fazio et al. 2004) and the Multiband Imaging Photometer for Spitzer (MIPS; Rieke et al. 2004) onboard the *Spitzer Space Telescope* (Werner et al. 2004) in 2006 November and 2007 February. These data are publicly available on IRSA<sup>3</sup>, where we retrieved the post-BCD (post Basic Calibrated Data) mosaics. They are directly used in the qualitative analysis of the distribution of dust and its spatial relation with molecular gas.

Archived data from the 2MASS Point Source Catalog (PSC) were also used in our work. To guarantee the reliability of the data, we adopted the source selection criteria from Li & Smith (2005). These include: a) each source extracted from the 2MASS PSC must have a certain detection in all  $J$ ,  $H$  &  $K_s$  wavebands; b) only sources with a  $K_s$ -band signal-to-noise ratio above 15 are selected. Young stellar object candidates were identified according to their 2MASS colour indices (e.g.,  $[J - H]$ , and  $[H - K_s]$ ). More details, see Sect. 3.4). The distribution of these potential YSOs and their relationship with other sources were investigated.

Photometric data of 6 IRAS point sources were retrieved from version 2.1 of IRAS Point Source Catalog. And their color indices and infrared luminosity are quantitatively investigated. Their relations with and effects to the molecular cloud are discussed in following analysis.

## 3 RESULTS

Figure 1 shows the  $^{13}\text{CO } J = 2 - 1$  and  $^{12}\text{CO } J = 3 - 2$  mapping grids of L1174 and its vicinity.  $^{13}\text{CO } J = 2 - 1$  spectra show mono-peak resembling gaussian profiles. In contrast, profiles of  $^{12}\text{CO } J = 3 - 2$  show complicated structures. This suggests that  $^{12}\text{CO } J = 3 - 2$  transition is optically thick in this region, while  $^{13}\text{CO } J = 2 - 1$  is relatively optically thin. Thus, the molecular gas traced with  $^{13}\text{CO } J = 2 - 1$  line is less affected by optical depth. We will use this line to derive the physical properties of the cloud.

### 3.1 Molecular cores

As shown in Figure 1 (a), the intensity of  $^{13}\text{CO}$  line varies throughout the region. This suggests a complex distribution of molecular gas on the projected plane of sky. There exists a cavity at the mid-west. And relatively denser gas is surrounding the cavity. In the following analysis, six molecular cores with different physical conditions are resolved.

<sup>1</sup> The KOSMA telescope has been transferred to Yangbajing, Tibet, China.

<sup>2</sup> <http://www.cfa.harvard.edu/gouldbelt/>

<sup>3</sup> NASA/IPAC Infrared Science Archive (IRSA) is part of the Infrared Processing and Analysis Center (IPAC), which is operated by the Jet Propulsion Laboratory, California Institute of Technology, under contract with the National Aeronautics and Space Administration. <http://irsa.ipac.caltech.edu/>

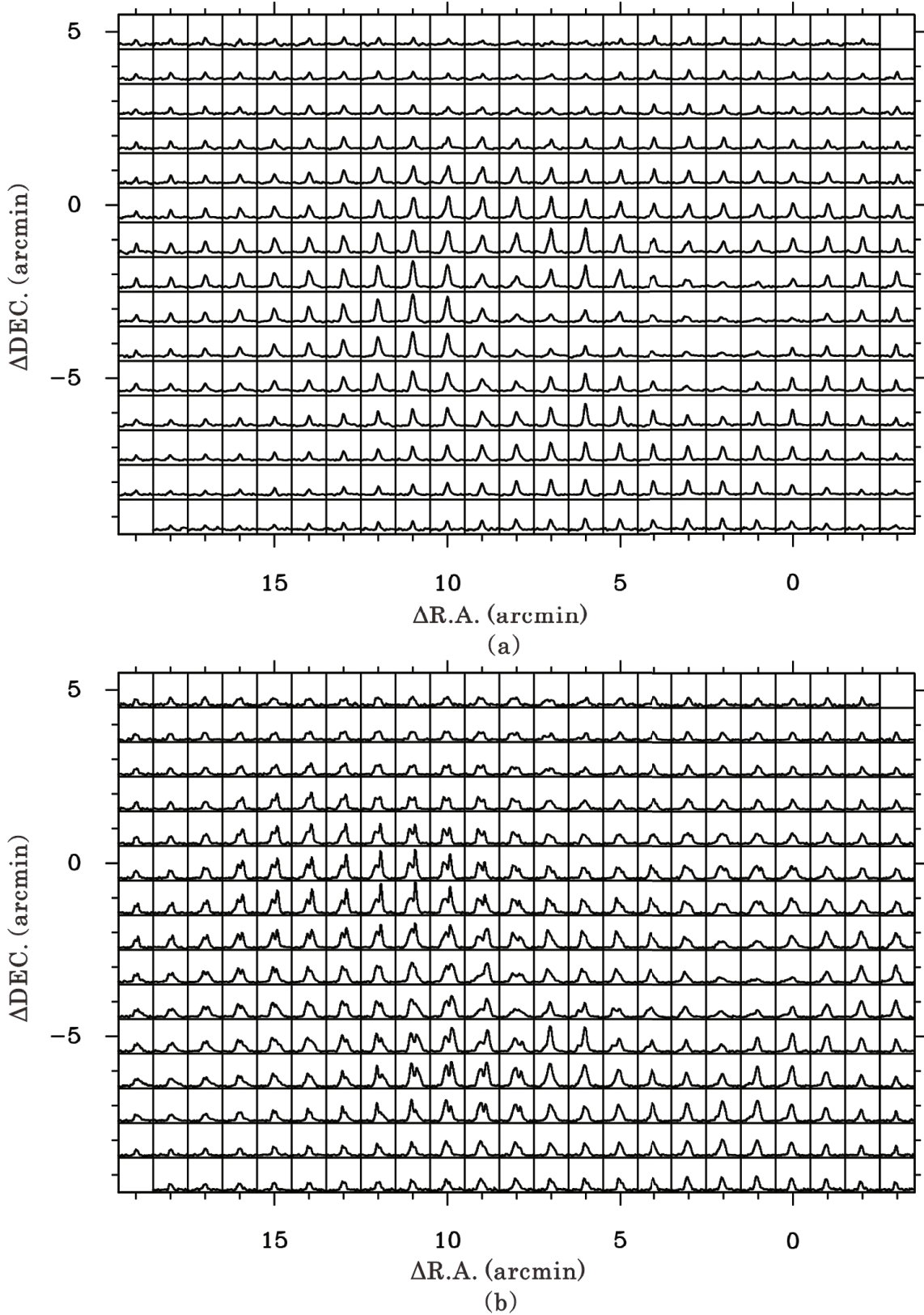


**Figure 1.** Mapping grids of L1174 and its vicinity. (a) For the line of  $^{13}\text{CO } J=2-1$ . The velocity range for each spectrum covers  $-5$  to  $10 \text{ km s}^{-1}$ , while the intensity ranges from  $-1$  to  $13 \text{ K}$ . (b) For the line of  $^{12}\text{CO } J=3-2$ . The velocity range for each spectrum is as the same as that in panel (a), while the intensity ranges from  $-1$  to  $6 \text{ K}$ .

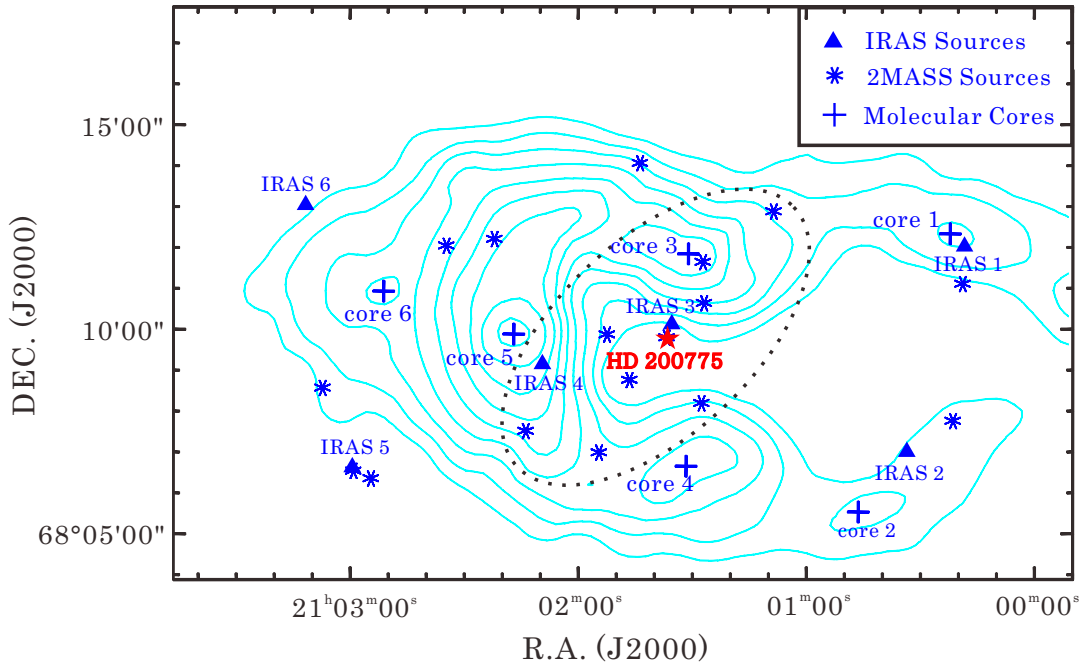


**Figure 2.** Velocity-integrated intensity map of  $^{13}\text{CO } J = 2 - 1$  emission. The velocity interval covers  $-2 \text{ km s}^{-1}$  to  $7 \text{ km s}^{-1}$ . The contour levels range from  $4.8$  to  $13.1 \text{ K km s}^{-1}$  with a step of  $1.5\sigma$  ( $1\sigma = 0.69 \text{ K km s}^{-1}$ ). The peak positions of the six molecular cores identified in this paper are labeled with crosses. The asterisks mark the candidate YSOs from 2MASS PSC, while the filled triangles indicate IRAS point sources in the field of view, whose corresponding identities are listed in Table 3. The red star represents the Herbig Be star HD 200775.

### 3.1.1 Identification

Figure 2 shows the velocity-integrated intensity map of  $^{13}\text{CO } J = 2 - 1$  rotational transition. We, by eye, identified six intensity peaks as cores, which are labeled as core 1 to core 6 with ascending right ascension order. The coordinates of the cores were converted from the offsets of intensity peaks to equatorial system (J2000) and are given in Table 1. The uncertainties of them are referred to the pointing error, which is better than  $10''$ . The radius of each core was determined according to the nearest point with 50% of its peak intensity and is presented in Table 2. We estimate that more than 80% of the masses of the cores are involved in spheres with these radii.

Core 1 to 5 are distributed surrounding a cavity, which has been excavated by an energetic and bipolar outflow in an earlier evolutionary stage of the massive Herbig Be star HD 200775 (Fuente et al. 1998). And core 6 is situated at the most east, about  $8'$  ( $\sim 1 \text{ pc}$ ) away from HD 200775. Core 1 is associated with IRAS 20597+6800, while core 3 is coincident with a 2MASS YSO candidate (2MASS J21013520+6810086). No IRAS point sources or 2MASS YSO candidates are detected at the near vicinities of the other four molecular cores. Core 3, core 4 and core 5 show notable intensity gradients at the directions towards HD 200775. This could be attributed to the feedbacks from the central Herbig Be star.

The spectra of  $^{13}\text{CO } J = 2 - 1$  and  $^{12}\text{CO } J = 3 - 2$  at the peak of each core are shown in Figure 3. Rotational line of  $^{13}\text{CO } J = 2 - 1$  shows similar mono-peak profiles at all six cores, while that of  $^{12}\text{CO } J = 3 - 2$  differs from each other. For core 1, line of  $^{12}\text{CO } J = 3 - 2$  indicates a blue-skewed profile and broad line wings. This line shows mono-peak with a blue wing at core 2 and 4, while weak blue-skewed profile feature at core 3 and 5. Contrast to core 1, a red-skewed profile is observed at core 6.

### 3.1.2 LTE parameters

To investigate the nature of the cores, it is firstly necessary to obtain estimates of some physical parameters, e.g., temperatures, masses. The derivation of these parameters follows a rotation temperature – column density analysis under the assumed conditions of local thermodynamic equilibrium (LTE) (Garden et al. 1991).

One component gaussian fittings to molecular lines at peaks of the cores were carried out. In Table 1, the antenna temperatures, velocity centroid, and full widths at half-maximum (FWHM) of lines of  $^{13}\text{CO } J = 2 - 1$  and  $^{12}\text{CO } J = 3 - 2$  are given.

According to Garden et al. (1991), under conditions of LTE, the measured main beam temperature  $T_{mb}$  and the column density of  $^{13}\text{CO } (N_{^{13}\text{CO}})$  can be expressed as follows,

$$T_{mb} = \frac{h\nu}{\kappa} \left[ \frac{1}{\exp(\frac{h\nu}{\kappa T_{ex}}) - 1} - \frac{1}{\exp(\frac{h\nu}{\kappa T_{bg}}) - 1} \right] \times [1 - \exp(-\tau)] f \quad (1)$$

$$N_{^{13}\text{CO}} = \frac{3\kappa}{8\pi^3 B\mu^2} \frac{\exp[hBJ(J+1)/\kappa T_{ex}]}{(J+1)} \times \frac{(T_{ex} + hB/3\kappa)}{[1 - \exp(-h\nu/\kappa T_{ex})]} \int \tau_{13} dv \quad (2)$$

where  $T_{ex}$  is the exciting temperature which we estimate to be about  $20 \pm 4 \text{ K}$  from the averaged dust temperature of the 6 IRAS sources (see Table 3),  $T_{bg} = 2.75 \text{ K}$  is the temperature of the cosmic background radiation,  $f$  is the beam-filling factor which is 1 in our observations,  $B$  and  $\mu$  are the rotational constant and permanent dipole moment of  $^{13}\text{CO}$ ,  $J$  is the rotational quantum number of the lower state in the observed rotational transition.

The combination of equation 1 and 2 would lead to a revised expression of  $N_{^{13}\text{CO}}$  as,

$$N_{^{13}\text{CO}} = \frac{3\kappa^2}{16\pi^3 \mu^2 h B^2} \frac{\exp[hBJ(J+1)/\kappa T_{ex}]}{(J+1)^2} \times \frac{(T_{ex} + hB/3\kappa)}{[1 - \exp(\frac{-h\nu}{\kappa T_{ex}})]}$$

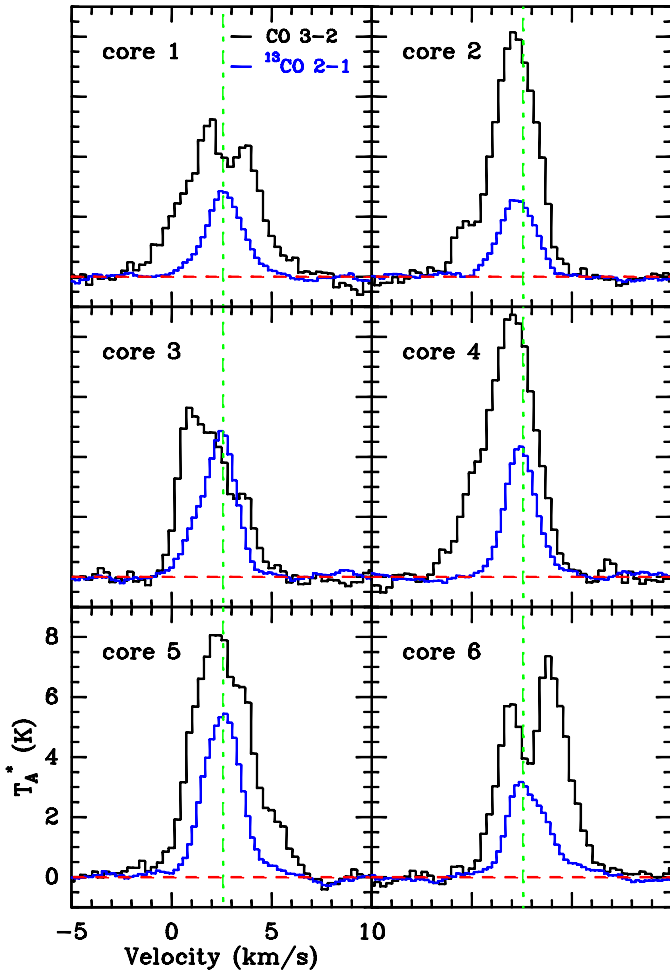


**Figure 3.** Profiles of  $^{13}\text{CO } J = 2 - 1$  and  $^{12}\text{CO } J = 3 - 2$  emission lines at the peaks of the six cores. The red dashed line shows the zero level intensity, while the green dash-dotted line indicates the system velocity  $V_{\text{sys}} = 2.58 \text{ km s}^{-1}$ .

$$\times \frac{1}{\left[ \frac{1}{\exp(h\nu/kT_{\text{ex}})-1} - \frac{1}{\exp(h\nu/kT_{\text{bg}})-1} \right]} \int T_{\text{mb}} \frac{\tau dv}{1 - \exp(-\tau)} \quad (3)$$

where  $\tau$  is the optical depth of  $^{13}\text{CO } J = 2 - 1$ . Given the optically thin feature of  $^{13}\text{CO } J = 2 - 1$  emission, the term  $\frac{\tau}{1 - \exp(-\tau)}$  is approximate 1. The velocity-integrated intensities  $\int T_{\text{mb}} dv$  for the cores are resulted from the gaussian fitting and given in Table 2. To obtain the column densities of molecular hydrogen  $N_{\text{H}_2}$ , we adopt a canonical  $[\text{CO}]/[\text{H}_2]$  abundance ratio of  $\approx 10^4$ , as measured in nearby molecular clouds (Frerking, Langer, & Wilson 1987; Pineda, Caselli, & Goodman 2008). Given the near distance of L1174, the isotope ratio  $[^{12}\text{C}]/[^{13}\text{C}]$  in the local ISM is applied, which is about 77 (Wilson & Rood 1994). With an assumed error of 10 percent for the isotope ratio, uncertainties are counted while deriving the  $N_{\text{H}_2}$ . The resulted column densities of  $^{13}\text{CO}$  and  $\text{H}_2$  are given in column 4 and 5 of Table 2.

The finally derived mass of each core is reached with an assumption of a homogenous sphere structure.

$$M_{\text{LTE}} = \frac{4}{3} \pi R^3 n_{\text{H}_2} \mu_g m(\text{H}_2) \quad (4)$$

where  $\mu_g = 1.36$  is the mean atomic weight of gas,  $m(\text{H}_2)$  is the mass of a hydrogen molecule, and  $n_{\text{H}_2} = N_{\text{H}_2}/2R$  is the number

density of molecular hydrogen. The resulted LTE masses of the six cores are presented in column 7 of Table 2. The masses vary from 4.9 to 31  $M_{\odot}$  with a median value of 14  $M_{\odot}$ .

### 3.1.3 Virial masses

To collapse for a core, the mass should be larger than its virial mass. We follow MacLaren, Richardson, & Wolfendale (1988) to estimate the virial masses of the cores with the assumption of constant density distributions.

$$\frac{M_{\text{vir}}}{M_{\odot}} = 210 \left( \frac{\Delta v}{\text{km s}^{-1}} \right)^2 \left( \frac{R}{\text{pc}} \right) \quad (5)$$

where  $\Delta v$  is the FWHM of the observed molecular line (see Table 1) and  $R$  the estimate of radius given in Table 2. Column 8 of Table 2 shows the resulted virial masses ranging from 171.2 to 463  $M_{\odot}$  which are evidently larger than the LTE masses.

## 3.2 $^{12}\text{CO } J = 3 - 2$ mapping

Figure 4 (a) shows the velocity-integrated intensity map of  $^{12}\text{CO } J = 3 - 2$  (contours) overlaid on that of  $^{13}\text{CO } J = 2 - 1$  (gray). The distribution of  $^{12}\text{CO}$  is more extended than that of  $^{13}\text{CO}$ . This is because that emissions from  $^{12}\text{CO}$  trace more diffuse and external part of molecular clouds. The positions of intensity peaks of  $^{12}\text{CO}$  are not consistent with that of cores traced by  $^{13}\text{CO}$ . Self-absorption of  $^{12}\text{CO } J = 3 - 2$  at densest region could explain this phenomenon. The large column density at the immediate vicinity of cores makes  $^{12}\text{CO } J = 3 - 2$  rotational line to be optically thick. This would cause deviation in the observed distribution of  $^{12}\text{CO}$ .

Another interesting feature from the observations is the diversity of profiles of  $^{12}\text{CO } J = 3 - 2$  line spectra (see Figure 1 (b)). Conspicuously asymmetric double-peaked spectral lines are detected in large area of this region. Such asymmetric double-peaked profiles are always regarded as effective tracers of kinematics of molecular clouds. Asymmetrically blue profiles, lines with the peaks skewed to the blue sides, are frequently interpreted as evidence of inward motions. Such inward motions could be collapse (Zhou et al. 1993; Evans et al. 2005) or infall (Wu & Evans 2003; Wu et al. 2005). By contrast, the red-asymmetry is observed when a centrally concentrated system (i.e., with excitation temperature decreasing outward) is expanding.

Figure 4 (b)–(d) show the spectral profiles of  $^{12}\text{CO } J = 3 - 2$  in three subregions labeled with red boxes in panel (a). Lines in subregion I, corresponding to core 1, show dominant blue profiles, which could be due to infall motions (see Sect. 4.1.1). In a relatively larger area (about 1 pc in diameter), red profiles are detected in subregion II. In our further analysis, this would be attributed to the global expansion rather than outflow (see Sect. 4.2). Much more complex line profiles are observed in subregion III, in which blue and red profiles show up alternately. The backflow of stellar winds and feedbacks from two potential 2MASS YSOs could induce complexity to the line profiles in subregion III (see Sect. 4.2).

## 3.3 Associated IRAS sources

There are 6 IRAS point sources detected in the mapping region of KOSMA observations. They are marked in Figure 2 and Figure 4 with filled triangles and labeled as IRAS 1 to 6 with ascending right ascension. Their genuine IRAS names and IRAS photometric data from the catalog are given in Table 3. As shown in Figure 2,

**Table 1.** Fitting parameters of cores.

Label	R.A. (J2000)	DEC. (J2000)	$^{13}\text{CO } (J=2-1)$			$\text{CO } (J=3-2)$		
			$T_A^*$ (K)	$v_{\text{LSR}}$ (km/s)	FWHM (km/s)	$T_A^*$ (K)	$v_{\text{LSR}}$ (km/s)	FWHM (km/s)
core 1	21:00:22.13	68:12:25.9	2.7395	2.638(0.014)	2.234(0.036)	5.2106	2.401(0.032)	3.974(0.083)
core 2	21:00:45.84	68:05:30.7	2.5911	2.287(0.014)	2.126(0.033)	7.9352	2.135(0.014)	2.656(0.035)
core 3	21:01:31.11	68:11:46.3	4.5975	2.363(0.014)	2.116(0.034)	5.3655	1.724(0.021)	3.077(0.046)
core 4	21:01:31.76	68:06:39.1	4.2942	2.439(0.009)	1.843(0.023)	8.4209	1.911(0.017)	3.049(0.040)
core 5	21:02:17.13	68:09:52.9	5.4667	2.543(0.010)	2.197(0.024)	7.9722	2.500(0.018)	3.437(0.042)
core 6	21:02:51.30	68:10:54.7	3.0554	2.765(0.015)	2.385(0.038)	9.3281	3.115(0.013)	3.080(0.041)

**Table 2.** Physical Parameters of cores.

Label	R (pc)	$\int T_{\text{mb}} dv$ (K km s $^{-1}$ )	$N_{^{13}\text{CO}}$ ( $10^{15}$ cm $^{-2}$ )	$N_{\text{H}_2}$ ( $10^{21}$ cm $^{-2}$ )	$n(\text{H}_2)$ ( $10^3$ cm $^{-3}$ )	$M_{\text{LTE}}$ ( $M_{\odot}$ )	$M_{\text{vir}}$ ( $M_{\odot}$ )	$P_{\text{ex}}/k$ ( $10^5$ K cm $^{-3}$ )
core 1	0.17	8.9(0.2)	4.9(0.2)	3.8(0.5)	3.6(1.0)	4.9(2.2)	174.3(28.1)	3.2(2.5)
core 2	0.18	8.0(0.1)	4.4(0.2)	3.4(0.5)	3.0(0.8)	5.0(2.1)	171.2(25.6)	2.5(1.8)
core 3	0.20	14.2(0.2)	7.8(0.3)	6.0(0.9)	4.8(1.2)	10.9(2.1)	187.6(26.1)	3.5(2.9)
core 4	0.26	11.5(0.1)	6.4(0.3)	4.8(0.7)	3.0(0.7)	15.0(1.8)	183.4(19.8)	1.5(0.7)
core 5	0.24	17.5(0.2)	9.7(0.4)	7.4(1.0)	5.0(1.1)	19.3(2.2)	247.7(26.9)	3.6(1.8)
core 6	0.39	10.6(0.1)	5.9(0.3)	4.5(0.6)	1.9(0.4)	31.0(2.4)	463.0(40.3)	1.7(0.6)

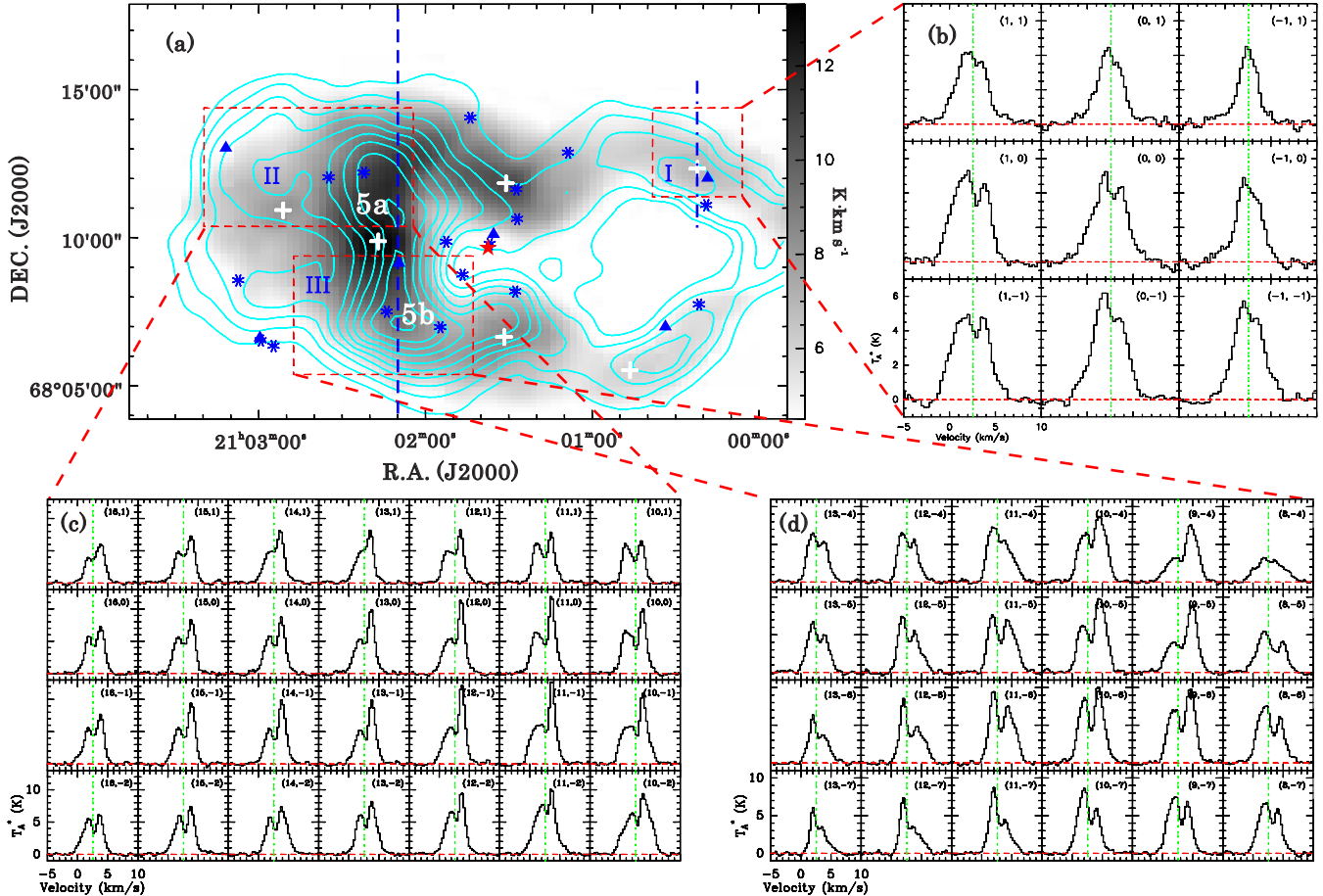


**Figure 4.** (a) Velocity-integrated intensity map of  $^{12}\text{CO } J=3-2$  (contours) overlaid on that of  $^{13}\text{CO } J=2-1$  (gray). The velocity interval covers  $-2$  km  $\text{s}^{-1}$  to  $7$  km  $\text{s}^{-1}$ . The contour levels range from  $14.6$  to  $39.3$  K km  $\text{s}^{-1}$  with a step of  $1.5\sigma$  ( $1\sigma = 1.83$  K km  $\text{s}^{-1}$ ). The red dashed boxes locate 3 subregions with complex line profiles. Other symbols are the same as the ones in Figure 2. (b) Line profiles of subregion I labeled in panel (a). The offsets are indicated at the up-right corner of each sub-panel. (c) The same as (b), but for subregion II. (d) The same as (b), but for subregion III.

**Table 3.** Properties of associated IRAS sources.

IRAS Name		$F_{12}$	$F_{25}$	$F_{60}$	$F_{100}$	$f_{qual}^a$	$\log(\frac{F_{25}}{F_{12}})$	$\log(\frac{F_{60}}{F_{12}})$	$L_{IR}$	$T_d^b$	2MASS Association
		(Jy)	(Jy)	(Jy)	(Jy)				( $L_{\odot}$ )	(K)	
IRAS 1	IRAS 20597+6800	0.250	0.823	4.48	55.13	1331	0.52	1.25	7.85	18.96	Null
IRAS 2	IRAS 20599+6755	0.677	0.595	18.98	1095.00	1231	-0.06	1.45	122.94	14.53	Null
IRAS 3	IRAS 21009+6758	26.660	76.770	637.70	1095.00	3333	0.46	1.38	364.98	31.02	J21013520+6810086
IRAS 4	IRAS 21015+6757	1.524	4.252	48.07	1095.00	3311	0.45	1.50	133.86	16.90	Null
IRAS 5	IRAS 21023+6754	0.266	0.387	0.40	15.46	3311	0.16	0.18	2.31	15.46	J21025943+6806322
IRAS 6	IRAS 21025+6801	0.357	0.796	10.66	25.17	3333	0.35	1.48	6.46	28.13	Null

<sup>a</sup> Flux density quality, 1 for an upper limit, 2 for moderate quality, and 3 for high quality. The four numbers for each source refer to the flux density quality of IRAS bands at 12, 25, 60 and 100  $\mu\text{m}$ , respectively.

<sup>b</sup> Dust temperatures were derived from color temperatures  $T_{c(60/100)}$  defined by Henning, Pfau, & Altenhoff (1990):  $T_d \approx T_{c(60/100)} = \frac{96}{(3+\beta)\ln(\frac{100}{60}) - \ln(\frac{F_{60}}{F_{100}})}$ .

IRAS 20597+6800 (IRAS 1 in this paper) and IRAS 21009+6758 (IRAS 3 in this paper) are associated with core 1 and HD 200775 respectively.

The infrared flux densities of the 6 IRAS sources are derived with the following equation (Casoli et al. 1986):

$$F(10^{-13}\text{Wm}^{-2}) = 1.75 \times \left( \frac{F_{12}}{0.79} + \frac{F_{25}}{2} + \frac{F_{60}}{3.9} + \frac{F_{100}}{9.9} \right), \quad (6)$$

where  $F_{12}$ ,  $F_{25}$ ,  $F_{60}$ , and  $F_{100}$  are the flux densities in Jy at 12  $\mu\text{m}$ , 25  $\mu\text{m}$ , 60  $\mu\text{m}$ , and 100  $\mu\text{m}$  respectively. With the distance of 440 pc, we obtain the infrared luminosity, which is given in column 10 of Table 3. Color indices of  $\log(\frac{F_{25}}{F_{12}})$  and  $\log(\frac{F_{60}}{F_{12}})$  are calculated and shown in Table 3 either.

Cross identification with 2MASS point source catalogue was performed for each IRAS source. The identification process followed the criteria of: a) an associated 2MASS point source must locate in the error ellipse of a IRAS source; b) the reddest one was selected if two or more 2MASS sources were found in the very near reaches of a IRAS source. None 2MASS associations were identified for IRAS 1, IRAS 2, IRAS 4 and IRAS 6. For IRAS 3, only one 2MASS source fulfills the first criterion and was determinately identified as the near-IR association. Two 2MASS point sources reside in the error ellipse of IRAS 5. The closer one possessing larger infrared color indices (i.e.,  $[J - H]$  and  $[H - K_s]$ ) was undoubtedly identified as the association. The results of the cross identification are given in column 12 of Table 3.

### 3.4 2MASS YSO candidates

Highly reliable 2MASS point sources were reexamined according to their colour indices (i.e.,  $[J - H]$ , and  $[H - K_s]$ ) to pick out the potential young stellar objects (YSOs). We dotted all the sources on the  $[J - H]$  vs.  $[H - K_s]$  diagram presented as Figure 5. The sources with colour indices fulfilling the relations of  $[J - H] < 1.8[H - K_s] - 0.103486$  and  $[H - K_s] > 0.5$  are regarded as YSOs (Li & Smith 2005). This process resulted in 17 YSO candidates in the mapping region of KOSMA observations. All of them are represented with red "+" in Figure 5. We numbered the 17 sources according to their distances to the Herbig Be star HD 200775, i.e., 2MASS 1 as the nearest one to HD 200775 and 2MASS 17 as the farthest. In Figure 2 and 4, they are marked with asterisks. Among the 17 YSO candidates, 3 ones were identified to be pre-main-sequence stars by Kun et al. (2009), and 11 ones were identified to be YSO candidates by Kirk et al. (2009). Photometri-

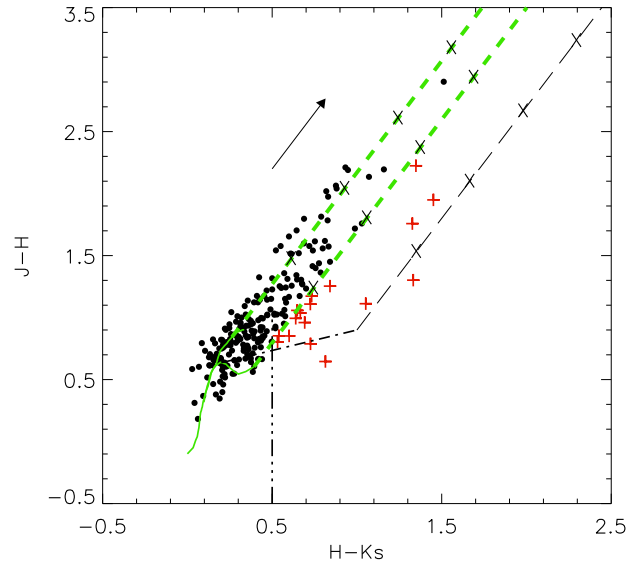


**Figure 5.**  $[J - H]$  vs.  $[H - K_s]$  diagram. The 17 YSO candidates are marked as red "+" (see Sect. 3.4 for details). Black dots represent 2MASS field stars which may be reddened main-sequence dwarfs and giants. The solid lines are the loci of the main-sequence dwarfs and giant stars (Bessell & Brett 1988). The arrow shows a reddening vector of  $A_V = 5$  mag (Rieke & Lebofsky 1985). The dot-dashed line indicates the locus of dereddened T Tauri stars (Meyer, Calvet, & Hillenbrand 1997). The dashed lines, which are drawn parallel to the reddening vector, define the reddening band for normal field stars and T Tauri stars. Crosses are over-plotted with an interval corresponding to  $A_V = 5$  mag.

cal data from the 2MASS catalogue and colour indices of all YSO candidates are given in column 3 to 8 of Table 4.

## 4 DISCUSSIONS

### 4.1 Molecular cores

#### 4.1.1 Evolutionary status

Diverse profiles of  $^{12}\text{CO } J = 3 - 2$  are detected in distinct cores. This, along with the distribution of the infrared sources (i.e., IRAS

**Table 4.** 2MASS YSO Candidates

	2MASS Name	$m_J$ (mag)	$m_H$ (mag)	$m_{K_s}$ (mag)	$J - H$ (mag)	$H - K_s$ (mag)	$J - K_s$ (mag)	$\alpha^*$	$D_{Angle}^*$ (armin)
2MASS 1 <sup>#</sup>	J21013691+6809476	6.111	5.465	4.651	0.65	0.81	1.46	0.47	0.00
2MASS 2 <sup>#†</sup>	J21012706+6810381	12.323	11.150	10.417	1.17	0.73	1.91	0.96	1.24
2MASS 3 <sup>#†</sup>	J21014672+6808453	11.792	10.798	10.159	0.99	0.64	1.63	0.95	1.38
2MASS 4 <sup>#</sup>	J21015265+6809520	14.062	13.004	12.356	1.06	0.65	1.71	1.00	1.47
2MASS 5	J21012774+6808114	13.999	13.195	12.663	0.80	0.53	1.34	0.94	1.82
2MASS 6 <sup>#</sup>	J21012734+6811383	15.378	13.154	11.806	2.22	1.35	3.57	0.96	2.05
2MASS 7	J21015475+6806590	14.116	13.264	12.664	0.85	0.60	1.45	0.87	3.26
2MASS 8 <sup>#</sup>	J21010870+6812525	14.736	13.627	12.902	1.11	0.73	1.83	0.92	4.05
2MASS 9 <sup>#</sup>	J21021404+6807306	15.768	14.656	13.604	1.11	1.05	2.16	0.62	4.14
2MASS 10 <sup>#</sup>	J21014391+6814033	15.036	13.734	12.402	1.30	1.33	2.63	0.57	4.31
2MASS 11	J21022228+6812121	16.434	15.180	14.339	1.25	0.84	2.10	0.89	4.86
2MASS 12	J21023492+6812024	15.337	14.377	13.685	0.96	0.69	1.65	0.84	5.84
2MASS 13	J21002149+6807452	17.019	15.261	13.934	1.76	1.33	3.09	0.77	7.30
2MASS 14	J21001891+6811062	15.386	14.533	13.994	0.85	0.54	1.39	0.98	7.37
2MASS 15 <sup>#</sup>	J21025484+6806210	15.661	13.712	12.261	1.95	1.45	3.40	0.78	8.02
2MASS 16 <sup>#†</sup>	J21025943+6806322	13.871	13.083	12.357	0.79	0.73	1.51	0.65	8.34
2MASS 17 <sup>#</sup>	J21030756+6808339	12.435	11.398	10.732	1.04	0.67	1.70	0.95	8.52

<sup>#</sup> Identified to be YSO candidate by Kirk et al. (2009).

<sup>†</sup> Identified to be pre-main-sequence star by Kun et al. (2009).

\* 2MASS *index* defined as  $\alpha = \frac{[J-H]}{1.8[H-K_s]-0.1035}$ , where  $[J-H]$  and  $[H-K_s]$  are 2MASS color indices. While  $\alpha = 1$ , a 2MASS point source will be located on the right dashed line in Figure 5 which is the locus dividing reddened normal field stars and T Tauri stars (Bessell & Brett 1988; Meyer, Calvet, & Hillenbrand 1997; Li & Smith 2005). An younger YSO would possess a smaller 2MASS index.

\* Angle distance to HD 200775.

source and 2MASS YSO candidates), suggests deferent evolutionary status of the cores.

**Core 1** is the smallest one in size. The association with IRAS 20597+6800 indicates ongoing star formation in core 1. The profile of  $^{12}\text{CO } J = 3 - 2$  shows blue-skewed asymmetric feature suggestive of infall motions. Based on the simple analytic model of radiative transfer proposed by Myers et al. (1996), the inward speed is estimated to be about  $0.43 \text{ km s}^{-1}$ . Shown in Figure 6 (a) is the position-velocity (P-V) diagram with a slice crossing the core 1 from north to south. This is a typical P-V diagram showing blue profile (Wu et al. 2007), which well resembles an infall scenario. Meanwhile, this P-V diagram indicates the detection of prominent line wings in core 1. Such feature is always interpreted as the result of outflow activities in star forming regions (Lada 1985). Point observation of L1174 (corresponding to core 1 in this study) in  $^{12}\text{CO } J = 1 - 0$  was performed by Wu, Zhou, & Evans (1992), and the prominent wing emission was interpreted as the evidence of the existence of an outflow. And in the outflow catalog of Wu, Huang, & He (1996), L1174 was classified as a source driving a bipolar outflow. Shown in Figure 6 (b) is the velocity-integrated intensity map of the wing emissions. The red lobe of the outflow is unambiguously revealed, while the blue lobe is not clear. Since core 1 is located in the large molecular envelope of HD 200775 whose feedback severely impacts the ambient material, it is difficult to separate the blue lobe of the outflow and the surrounding gas.

**Core 2** is the lightest one in mass. The  $^{12}\text{CO } J = 3 - 2$  line of core 2 shows mono-peak feature. This core is relatively diffuse. No IRAS source or 2MASS YSO candidate is detected in core 2. All these are suggestive of an evolutionary stage prior to the beginning of star formation.

**Core 3** is associated with a potential YSO 2MASS J21012734+6811383 (i.e., 2MASS 6 in this paper). This 2MASS source possesses large infrared excess ( $[J-H] = 2.22$ ,  $[H-K_s] = 1.35$ ) indicative of deeply embedded feature and an early evolutionary stage. The line of  $^{12}\text{CO } J = 3 - 2$  shows non-gaussian profile with the peak skewed to the blue end. This may be attributed to potential infall motions. As shown in Figure 2, the southern portion of this core is compressed by the feedback of HD 200775.

**Core 4** shows a mono-peak profile in  $^{12}\text{CO } J = 3 - 2$ . The density is as low as that of core 2. The lack of infrared source in this core suggests a similar evolutionary stage as core 2.

**Core 5** is the densest one. The large gradient in Figure 2 indicates that core 5 is heavily compressed by the winds from HD 200775. In the observations with  $^{12}\text{CO } J = 3 - 2$ , this core is resolved into two cores (see Figure 4). An IRAS source (i.e., IRAS 21015+6757) is located between core 5a and 5b. Core 5b is associated with 2MASS J21021404+6807306 (i.e., 2MASS 9 in this paper). Compared with 2MASS 6, 2MASS 9 shows smaller infrared excess ( $[J-H] = 1.11$ ,  $[H-K_s] = 1.05$ ). This indicate that core 5b could be more evolved than core 3. Shown in Figure 7 (a) is a position-velocity diagram along centers of the core 5a and 5b. This is a typical P-V diagram showing red profile (Wu et al. 2007). Both of the two cores show notable red-skewed asymmetric profiles (see Figure 7 (b)). These features could be ascribed to the global expansion originated from the feedback of HD 200775 (see Sect. 4.2).

**Core 6** is the largest, most massive and diffuse one. The line of  $^{12}\text{CO } J = 3 - 2$  at the peak of this core shows red-skewed asymmetric profile. No infrared source is detected in this core. This, combined with the diffuse feature, suggests that this core is in a very early stage. As shown in Figure 4, core 6 resides in the subregion II where red-skewed lines dominate. The origin of red-skew profile



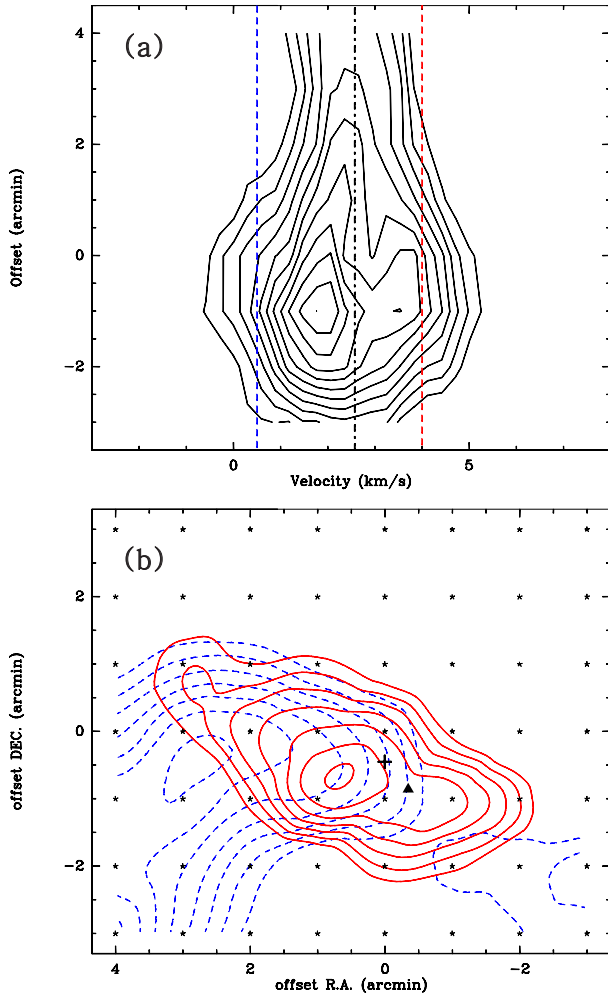


**Figure 6.** (a)  $^{12}\text{CO } J = 3 - 2$  position-velocity diagram constructed along the vertical dash-dotted line (*cross the core 1 from north to south*) in Figure 4 (a). The contour levels start from the 20% of the peak intensity with a step of 8%. And the peak intensity is 6.18 K. The vertical dash-dotted line indicates the system velocity  $V_{\text{sys}} = 2.58 \text{ km s}^{-1}$ . The two dashed lines indicate the beginning of the blue and red wings. (b) Velocity-integrated intensity map of wing emissions of  $^{12}\text{CO } J = 3 - 2$ . The velocity interval covers -1 to  $0.5 \text{ km s}^{-1}$  for the blue wing (*dashed lines*), while 4 to  $6 \text{ km s}^{-1}$  for the red wing (*solid lines*). The contour levels start from  $1.95 \text{ K km s}^{-1}$  with an increasing step of  $0.37 \text{ K km s}^{-1}$  for the blue wing and start from  $2.11 \text{ K km s}^{-1}$  with an increasing step of  $0.33 \text{ K km s}^{-1}$ . The cross presents the center of core 1, and the filled triangle indicates the location of IRAS 20597+6800 (IRAS 1 in this paper).

of  $^{12}\text{CO } J = 3 - 2$  in core 6 could be due to the global expansion (See Sect. 4.2).

#### 4.1.2 Potential collapse

Compared with that in other low-mass star forming regions (e.g., case in Taurus, Onishi et al. 2002), the line widths of cores in our observations are relatively large, ranging from  $1.8 \text{ km s}^{-1}$  in core 4 to  $2.4 \text{ km s}^{-1}$  in core 6 (FWHM of  $^{13}\text{CO } J = 2 - 1$  line). In regions with temperatures of about 20 K (see Table 3), the isothermal sound speeds would be about  $0.27 \text{ km s}^{-1}$  (McKee & Tan 2003). This is much smaller than the observed line widths. Therefore, some other non-thermal motions play dominant roles in the broadening of lines in this region. Several sources could be responsible for these non-

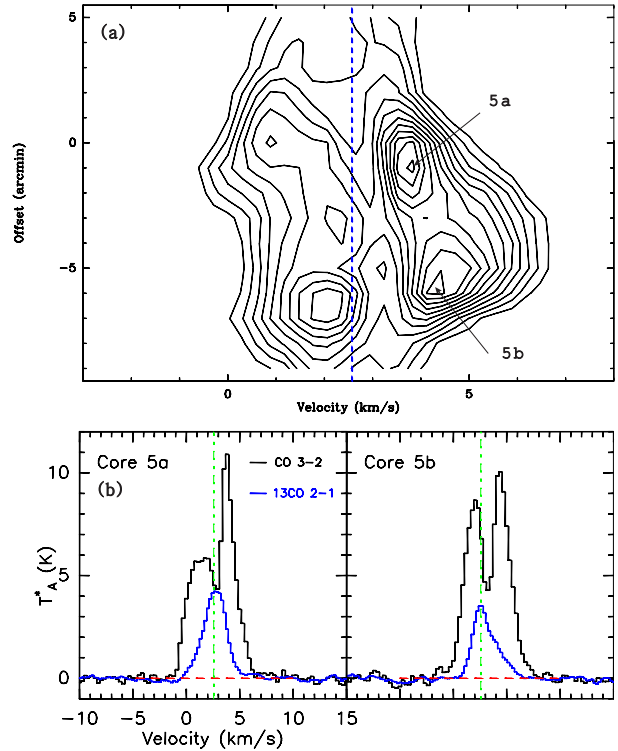


**Figure 7.** (a)  $^{12}\text{CO } J = 3 - 2$  position-velocity diagram constructed along the vertical dashed line in Figure 4 (a). The contour levels start from the 15% of the peak intensity with a step of 7.5%. And the peak intensity is 10.90 K. The vertical dashed line indicates the system velocity  $V_{\text{sys}} = 2.58 \text{ km s}^{-1}$ . (b) Profiles of  $^{13}\text{CO } J = 2 - 1$  and  $^{12}\text{CO } J = 3 - 2$  at the peaks of core 5a and 5b.

thermal line widths. One of them is that the cores formed in a turbulent environment and they are still turbulent (Saito et al. 2006). Meanwhile, some motions after the formation of a central protostar would lead to large line widths. Such motions could be infall, outflows, winds, and rotations (Pavlyuchenkov et al. 2008; Wu et al. 2005). Bulk motions due to central protostar may play key roles in the case of core 1 and core 3, especially in core 1, where infall of material is detected (see Sect. 4.1.1). Without associated infrared sources, the other four cores should be in turbulent conditions.

From the calculation performed in Sect. 3.1, one can see that the derived virial masses largely exceed the LTE masses for all six cores. This suggests that there isn't sufficient gravitational energy to bind the systems. Lee et al. (2011) and Wang et al. (2008) obtained similar LTE and virial masses in IRAS 05345+31571 and MWC 1080 star forming regions. Saito et al. (2006) also concluded that non-turbulent cores have similar virial masses to LTE masses but the virial masses are usually larger than the LTE masses for turbulent cores. External pressure is needed for a turbulent core to maintain a bound system.

We follow Saito et al. (2006) to estimate the least external pressures for the  $^{13}\text{CO}$  cores to be in bound systems. The virial equation will be amended to be as following with external pressure:

$$F = 2U + \Omega - 4\pi R^3 P_{\text{ex}} \quad (7)$$

where  $U = \frac{1}{2}M\sigma^2$  ( $\sigma$ -velocity dispersion) is the kinetic energy,  $\Omega = -\frac{3GM^2}{5R}$  is the gravitational energy, and  $R$  is the radius of the core. The velocity dispersion is deduced from the line width of

$^{13}\text{CO}$  using the equation of  $\sigma = \Delta v/2 \sqrt{2 \ln(2)}$ . While  $F = 0$ , we get the lower limits of the required external pressure. The results are then divided by Boltzmann constant  $\kappa$  and tabulated in Table 2. Notice that all the six cores need external pressures of  $P_{ex}/k \sim 10^5 \text{ K cm}^{-3}$  to maintain bound systems.

McKee & Tan (2003) suggested that the pressure at the surface of a core is related to its surface density:

$$P_{s,core} = 0.85 \times 10^9 \Sigma^2 \text{ K cm}^{-3} \quad (8)$$

where  $\Sigma = 1.36 N_{H_2} m(H_2)$  is the surface density in  $\text{g cm}^{-2}$ . In our case, the resulted surface pressure for all the six cores is about  $10^5 \text{ K cm}^{-3}$ , which is commensurate with the required external pressure for maintaining bound systems. In addition, winds from the central bright Herbig Be star HD 200775 would provide supplemental pressure to help binding the neighbour cores, i.e., core 3, core 4, and core 5. Therefore, we suggest that these turbulent cores can be bound with external pressure.

As discussed above, turbulence plays great role in balancing the gravitational force in the cores. However, previous studies showed that this support would not exist long enough to prevent them collapsing. This could be attributed to the relatively short dissipation timescale for turbulent motions, which is about  $\sim 10^5 \text{ yr}$ , much shorter than the free-fall timescale of  $\sim 10^6 \text{ yr}$  for a core with  $n_{H_2} \sim 10^3 \text{ cm}^{-3}$  (McKee & Ostriker 2007). This, along with the available surface pressure and feedbacks from HD 200775, suggests the six molecular cores resolved by our observations have the potential to collapse to form stars.

## 4.2 Global motions

Comparison of spectra of subregion *I* (Figure 4 (*b*)) with subregions *II* and *III* (Figure 4 (*c*) and (*d*)) evidently shows variation of line profile. Obviously, the line centers for the western subregion *I* are slightly blue-shifted with respect to the system velocity, while red-shifted for the eastern subregions *II* and *III*. This velocity variation is also detected with  $^{13}\text{CO } J = 2 - 1$  line emission. The velocity centroid shows a tendency of increasing with ascending right ascension (J2000) for the six cores (see Table.1). In Figure 8, the distribution of velocity centroid for the line of  $^{13}\text{CO } J = 2 - 1$  is presented and systematic velocity variation is confirmed. The value of the velocity gradient is estimated to be about  $0.94 \text{ km s}^{-1} \text{ pc}^{-1}$ , which is consistent with the result in Goodman et al. (1993). This could be due to the strong stellar wind from HD 200775 which is the brightest source in this region. On the other hand, this velocity gradient may suggest a scenario of cloud rotation with a NW-SE direction, while the southeast portion moving away from us and the northwest portion to us.

Feedbacks from stars with masses  $\geq 8 M_{\odot}$  would profoundly affect the conditions of the natal clouds. The strong radiation pressure and stellar winds could destroy the clouds to constraint further star forming activities, otherwise they may help dense cores form in surroundings which will collapse to form new generation stars (see Sect.4.3). In this work, HD 200775, a Herbig Be star with mass of  $\sim 10 M_{\odot}$ , would generate violent winds blowing the whole molecular cloud to globally expand. The powerful stellar winds or outflow from this young star blew away ambient material and excavate a cavity at the west where the density was relatively low. The dispersed material accumulated around the cavity to form filamentary structures where core 1 and core 2 have formed. For the portion to the east of HD 200775, large amount gas and high density prevent it being blown about. However, the winds still possibly make the whole molecular to be globally expanding.

Another observational evidence supporting a scenario of global expansion comes from the line profiles of  $^{12}\text{CO } J = 3 - 2$ . As shown in Figure 1 (*b*), red-skewed profiles dominates in spectra with two peaks. As mentioned in Sect.3.2, this is due to self-absorption of the molecular cloud with motions. Extensive red-skewed spectra can be observed in regions with expansion or inclined outflows. In our observations, the distribution of the red-skewed lines is more consistent with the situation of expansion. Given the fact that an outflow always has lobes constrained within certain directions, red-dominated profiles originated from an inclined outflow would be located in a region with relatively small opening angle and better collimation. In a scenario of an expanding molecular cloud with a hot bright star inside, the blue-shifted emission originate from the hemisphere closer to the observer while the red-shifted emission from the hemisphere farther away; for the excitation of the molecules is the highest near the hot star, the observer is always looking at the cooler side of the blue hemisphere and the hotter side of the red hemisphere; thus, the red emission should always be as strong as, or stronger than, the blue emission (an analogue to the scenario of collapsing core proposed by Zhou et al. (1993)).

However, not all lines of  $^{12}\text{CO } J = 3 - 2$  emission resemble the red-skewed profiles. This ostensibly conflict with the expansion scenario. Blue-skewed spectra, rather than red-skewed ones, dominates at the northwest (see Figure 1 and 4). This could be due to the infall motions in core 1 as aforementioned. The  $^{12}\text{CO } J = 3 - 2$  spectra detected at the southwest show mono-peak with relatively large wing emissions (see Figure 1 (*b*)). This indicates that the gas column density is pretty low. Thus the line of  $^{12}\text{CO } J = 3 - 2$  here is optically thin while compared with the one in other places in this region. Another confusion comes from the complicated spectra in subregion *III* as shown in Figure 1, where blue- and red-skewed line profiles are alternatively detected. Other mechanisms are necessary to destroy the homogeneity of  $^{12}\text{CO } J = 3 - 2$  line spectra. The blue-skewed profiles observed in the first column from right in Figure 4 (*d*) could be due to the backflow of stellar wind. To the southeast of the cloud, there are two 2MASS YSO candidates, 2MASS 15 (2MASS J21025484+6806210) and 2MASS 16 (2MASS J21025943+6806322, associated with IRAS 5). As shown in Figure 2 and 4 (*a*), the cloud is as if compressed by the feedback from these infrared sources. With particularly large infrared excessive emission, 2MASS 15 could be in an early evolutionary stage with possible outflow activities which may contribute to the occurrence of the blue-skewed profiles in the left three columns in Figure 4 (*d*).

## 4.3 Triggered star formation

Shown in Figure 9 is a close up view of the central part of the region. Gray scaled background with an inverted color map presents  $4.5 \mu\text{m}$  emission which mainly originate from  $\text{H}_2(v = 0 - 0, s(9, 10, 11))$  and  $\text{CO}(v = 1 - 0)$  in shocked regions or outflows (Smith et al. 2006; Davis et al. 2007; Cyganowski et al. 2008). Evidently shocked structures are resolved at north and south of HD 200775. It is believed that supersonic stellar winds and/or outflow originated from HD 200775 have been serving as the engine of these shocks. Relatively weak extended  $4.5 \mu\text{m}$  emission were detected in the east reaches. Nearby IRAS 4 (i.e., IRAS 21015+6757), an elongated structure still can be identified. This would be a trail feature of earlier shocks. For this region, we recommend a scenario of intermittent shocks generated by stellar winds from HD 200775.

Overlaid contours on  $4.5 \mu\text{m}$  emission in Figure 9 present

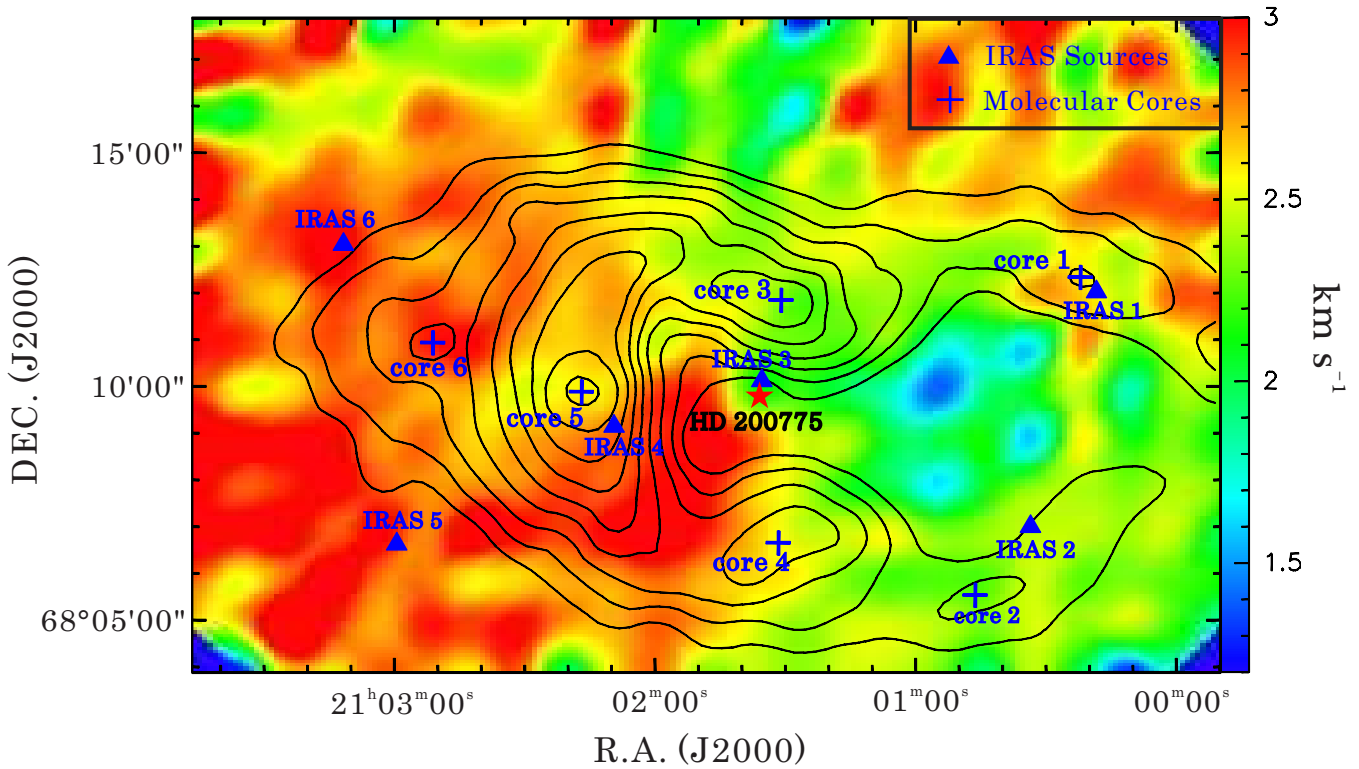


Figure 8. Distribution of line centroid of  $^{13}\text{CO } J = 2 - 1$ . The overlaid contours are as the ones in Fig.2.

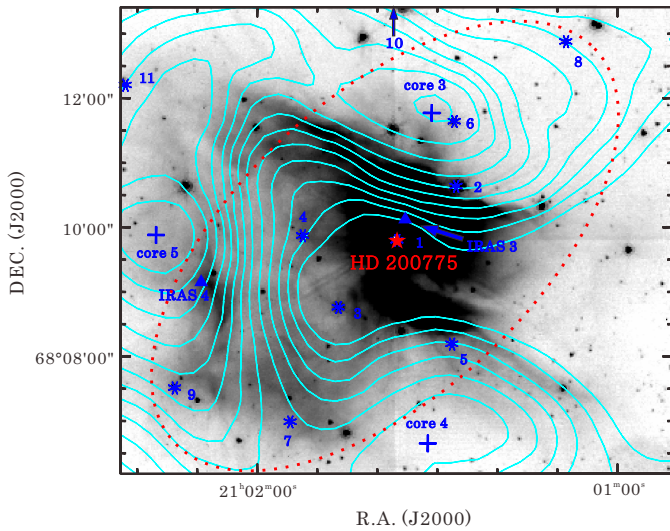


Figure 9. Close up view of the central part of the L 11174 region. The gray scaled background with a inverted color map presents the  $4.5 \mu\text{m}$  emission observed with PACS on *Spitzer*. The contours shows the velocity-integrated intensity of  $^{13}\text{CO } J = 2 - 1$ . The crosses, filled triangles, and asterisks indicate the molecular cores, IRAS sources, and 2MASS YSO candidates respectively. The bright Herbig Be star HD 200775 is marked with a red star. The dotted ellipse encircles the 9 YSO candidates nearest to HD 200775. These potential YSOs are aligned in NW-SE direction.

velocity-integrated intensity map of  $^{13}\text{CO } J = 2 - 1$  which roughly represents density distribution of gas. One can see large intensity gradients in sides toward HD 200775 for core 3, 4, and 5 which are located in sites closely surrounding HD 200775. These steep

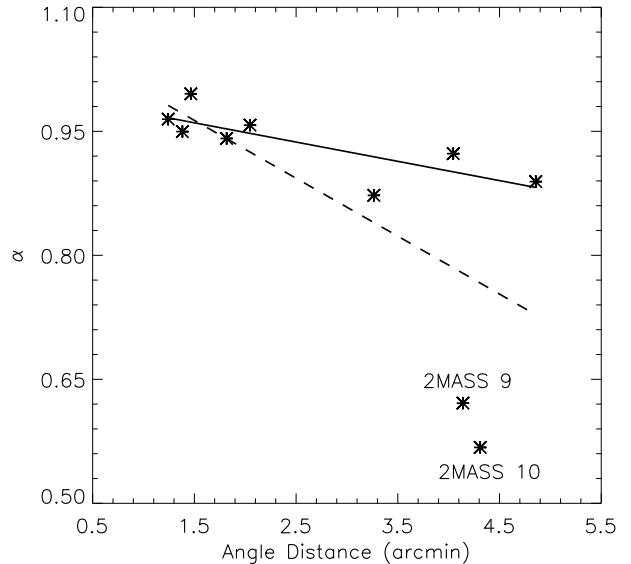


Figure 10. 2MASS index as a function of the angle distance to HD 200775 for the central 10 YSO candidates.

increases of intensities from HD 200775 to the near cores could be due to the strong winds from the bright Herbig Be star. Fierce winds have been enhancing gas density around HD 200775 to help form cores which would collapse to form new generation stars. If this is the case, one would expect to see a sharp velocity gradient around the shell excavated by HD 200775. As one can see in Figure 8, the velocity gradient increases some around HD 200775, but not

sharply. This could be due to the poor spatial resolution of our observation. The beam of  $80''$  would smooth the velocity difference in 0.2 pc.

Ten 2MASS YSO candidates (i.e., 2MASS 1-9 and 11) are marked with blue asterisks in Figure 9. They are labeled with numbers with increasing distances from HD 200775. Note that the nearest nine ones are aligned in NW-SE direction consistent with the velocity gradient shown in Figure 8. These features are suggestive of a scenario of triggered star formation in this region.

We define 2MASS *index* for a 2MASS source as,

$$\alpha = \frac{[J - H]}{1.8[H - K_s] - 0.1035} \quad (9)$$

where  $[J - H]$  and  $[H - K_s]$  are 2MASS color indices. 2MASS indices for all 17 YSO candidates were calculated and tabled in column 9 of Table 4. With an  $\alpha = 1$ , a 2MASS point source will locate on the right dashed line in Figure 5 which is the dividing line between reddening normal field stars and T Tauri stars (Bessell & Brett 1988; Meyer, Calvet, & Hillenbrand 1997; Li & Smith 2005). A younger YSO would possess a smaller 2MASS index.

We dotted the 10 2MASS YSO candidates nearest to HD 200775 (i.e., 2MASS 2-11, with exclusion of 2MASS 1 which is the 2MASS association of HD 200775) on a plot of 2MASS index vs. angle distance to HD 200775 (see Figure 9). A tendency of decreasing of  $\alpha$  with increasing angle distance is presented. To quantitatively evaluate the existence of such inverse correlation, we performed least square linear fitting. Presented as a dashed line is the fitted result with all ten points. This is representative a linear equation of  $\alpha = (-0.070 \pm 0.028)d + (1.068 \pm 0.089)$ , where  $d$  is the angle distance to HD 200775 from a 2MASS YSO candidate. This indicates that the more aged YSOs, with larger 2MASS index  $\alpha$ , resides closer to HD 200775 and younger ones farther away. However, a modest correlation coefficient of  $R^2 = 0.44$  indicate that this tendency is not highly reliable. Shown as a solid line in Figure 9, another fitting without considering 2MASS 9 and 10, which possess extremely small 2MASS indices, results in a linear equation of  $\alpha = (-0.023 \pm 0.007)d + (0.995 \pm 0.021)$  and a larger correlation coefficient of  $R^2 = 0.62$ . Intriguingly, the tendency of descending  $\alpha$  (i.e., decreasing age) with increasing angle distance is better confirmed. This feature is reminiscent of sequential star formation which is always interpreted as evidence of triggered star formation in the literature (Elmegreen & Lada 1977; Preibisch & Zinnecker 2007).

## 5 SUMMARY

We carried out mapping observations of L1174 in lines of  $^{13}\text{CO } J = 2 - 1$  and  $^{12}\text{CO } J = 3 - 2$  at 220.399 GHz and 345.796 GHz. Based on observed and archival data, the molecular conditions and star forming activities in L1174 were extensively investigated.

Six molecular cores are resolved by the observations in  $^{13}\text{CO } J = 2 - 1$ . Local thermodynamic equilibrium based calculations resulted in core masses of 5 to  $31 M_{\odot}$  with an median value of  $15 M_{\odot}$ . Relatively large line width in all six cores indicates turbulent motions throughout the L1174 region. This also leads to large virial masses ranging from  $171.2$  to  $463 M_{\odot}$ , a factor of magnitude higher than the LTE masses. However, these cores are still possible to collapse to form new stars given the available external pressure and the affects from the bright Herbig Be star HD 200775.

Conspicuously asymmetric line profiles of  $^{13}\text{CO } J = 2 - 1$

spectra are observed in a large area in L1174, which indicates bulk motions in this star forming region. Purely blue-skewed line features detected in core 1 suggest the existence of infall motions. Prominent wing emissions imply potential outflows in L1174 which are not resolved because of the low resolution of our observations.

Extensive red-skewed line features are detected to the east of HD 200775. This, together with the velocity gradient along NW-SE direction, indicates global expansion in L1174. Formed in the natal cloud, HD 200775 generated strong winds that blew away ambient material and excavated a cavity at the west where the density was relatively low. For the portion in the east, large amount of gas and high density prevent it from dispersing. And the consequence of the interaction between the winds and the gas is the global expansion of the reconstructed cloud.

Seventeen YSO candidates were identified according to 2MASS colour indices. For the ten 2MASS YSO candidates nearest to HD 200775, a tendency of decreasing age with increasing distance to HD 200775 is detected. This, along with large  $^{13}\text{CO}$  intensity gradient of cores near HD 200775 and the shock features observed at  $4.5 \mu\text{m}$ , suggests a scenario of star formation triggered by the Herbig Be star HD 200775.

## ACKNOWLEDGMENTS

We thank the referee Paola Caselli for constructive comments that helped us improve this paper. This project is supported by the National Natural Science Foundation of China through grant NSFC 11073027, the China Ministry of Science and Technology through grants 2012CB821800 (a State Key Development Program for Basic Research) and 2010DFA02710 (by the Department of International Cooperation).

## REFERENCES

- Abergel A., et al., 2010, *A&A*, 518, L96
- Alecian E., et al., 2008, *MNRAS*, 385, 391
- Allen L., Spitzer Gould Belt Legacy Team, 2007, *BAAS*, 38, 881
- An J. H., Sellgren K., 2003, *ApJ*, 599, 312
- Benson P. J., Caselli P., Myers P. C., 1998, *ApJ*, 506, 743
- Berné O., Joblin C., Rapacioli M., Thomas J., Cuillandre J.-C., Deville Y., 2008, *A&A*, 479, L41
- Bessell M. S., Brett J. M., 1988, *PASP*, 100, 1134
- Boersma C., Bauschlicher C. W., Allamandola L. J., Ricca A., Peeters E., Tielens A. G. G. M., 2010, *A&A*, 511, A32
- Bontemps S., Andre P., Terebey S., Cabrit S., 1996, *A&A*, 311, 858
- Buckle J. V., Fuller G. A., 2002, *A&A*, 381, 77
- Butner H. M., Lada E. A., Loren R. B., 1995, *ApJ*, 448, 207
- Casoli F., Combes F., Dupraz C., Gerin M., Boulanger F., 1986, *A&A*, 169, 281
- Cyganowski C. J., et al., 2008, *AJ*, 136, 2391
- Davis C. J., Kumar M. S. N., Sandell G., Froebrich D., Smith M. D., Currie M. J., 2007, *MNRAS*, 374, 29
- Elmegreen B. G., Lada C. J., 1977, *ApJ*, 214, 725
- Evans N. J., II, Lee J.-E., Rawlings J. M. C., Choi M., 2005, *ApJ*, 626, 919
- Fazio G. G., et al., 2004, *ApJS*, 154, 10
- Frerking M. A., Langer W. D., Wilson R. W., 1987, *ApJ*, 313, 320

- Fuente A., Martin-Pintado J., Rodriguez-Franco A., Moriarty-Schieven G. D., 1998, *A&A*, 339, 575
- Fuller G. A., Myers P. C., 1993, *ApJ*, 418, 273
- Furuya R. S., Kitamura Y., Wootten A., Claussen M. J., Kawabe R., 2003, *ApJS*, 144, 71
- Garden R. P., Hayashi M., Hasegawa T., Gatley I., Kaifu N., 1991, *ApJ*, 374, 540
- Graf U. U., Haas S., Honingh C. E., Jacobs K., Schieder R., Stutzki J., 1998, in Phillips T. G., ed., *Proc. SPIE Vol. 3357, Advanced Technology MMW, Radio, and Terahertz Telescopes*, p. 159
- Goodman A. A., Benson P. J., Fuller G. A., Myers P. C., 1993, *ApJ*, 406, 528
- Habart E., Abergel A., Boulanger F., Joblin C., Verstraete L., Compiègne M., Pineau Des Forêts G., Le Bourlot J., 2011, *A&A*, 527, A122
- Harju J., 1989, *A&A*, 219, 293
- Henning T., Pfau W., Altenhoff W. J., 1990, *A&A*, 227, 542
- Hernández J., Calvet N., Briceño C., Hartmann L., Berlind P., 2004, *AJ*, 127, 1682
- Joblin C., et al., 2010, *A&A*, 521, L25
- Kirk J. M., et al., 2009, *ApJS*, 185, 198
- Kun M., Balog Z., Kenyon S. J., Mamajek E. E., Gutermuth R. A., 2009, *ApJS*, 185, 451
- Kun M., Kiss Z. T., Balog Z., 2008, in Reipurth B., ed., *Handbook of Star Forming Regions, Volume I: The Northern Sky*, ASP Monograph Publications, P. 136
- Lada C. J., 1985, *ARA&A*, 23, 267
- Lee K. I., Looney L. W., Klein R., Wang S., 2011, *MNRAS*, 415, 2790
- Li J. Z., Smith M. D., 2005, *ApJ*, 620, 816
- Lynds B. T., 1962, *ApJS*, 7, 1
- MacLaren I., Richardson K. M., Wolfendale A. W., 1988, *ApJ*, 333, 821
- Madden S. C., Irvine W. M., Swade D. A., Matthews H. E., Friberg P., 1989, *AJ*, 97, 1403
- McKee C. F., Ostriker E. C., 2007, *ARA&A*, 45, 565
- McKee C. F., Tan J. C., 2003, *ApJ*, 585, 850
- Meyer M. R., Calvet N., Hillenbrand L. A., 1997, *AJ*, 114, 288
- Monnier J. D., et al., 2006, *ApJ*, 647, 444
- Myers P. C., Heyer M., Snell R. L., Goldsmith P. F., 1988, *ApJ*, 324, 907
- Myers P. C., Linke R. A., Benson P. J., 1983, *ApJ*, 264, 517
- Myers P. C., Mardones D., Tafalla M., Williams J. P., Wilner D. J., 1996, *ApJ*, 465, L133
- Onishi T., Mizuno A., Kawamura A., Tachihara K., Fukui Y., 2002, *ApJ*, 575, 950
- Okamoto Y. K., et al., 2009, *ApJ*, 706, 665
- Pavlyuchenkov Y., Wiebe D., Shustov B., Henning T., Launhardt R., Semenov D., 2008, *ApJ*, 689, 335
- Persi P., Palagi F., Felli M., 1994, *A&A*, 291, 577
- Pety J., 2005, in Casoli F., Contini T., Hameury J. M., & Pagani L., eds., *SF2A-2005: Semaine de l'Astrophysique Française*, EdP-Sciences, p. 721,
- Pineda J. E., Caselli P., Goodman A. A., 2008, *ApJ*, 679, 481
- Preibisch T., Zinnecker H., 2007, in Elmegreen B. G., Palous J., eds., *Proc. IAU Symp. 237, Triggered Star Formation in a Turbulent ISM*, Cambridge University Press, p. 270
- Rieke G. H., Lebofsky M. J., 1985, *ApJ*, 288, 618
- Rieke G. H., et al., 2004, *ApJS*, 154, 25
- Rosenberg M. J. F., Berné O., Boersma C., Allamandola L. J., Tielens A. G. G. M., 2011, *A&A*, 532, A128
- Saito H., Saito M., Moriguchi Y., Fukui Y., 2006, *PASJ*, 58, 343
- Sellgren K., Uchida K. I., Werner M. W., 2007, *ApJ*, 659, 1338
- Sellgren K., Werner M. W., Ingalls J. G., Smith J. D. T., Carleton T. M., Joblin C., 2010, *ApJ*, 722, L54
- Schieder R., Tolls V., Winnewisser G., 1989, *Experimental Astronomy*, 1, 101
- Smith H. A., Hora J. L., Marengo M., Pipher J. L., 2006, *ApJ*, 645, 1264
- Straizys V., Cernis K., Kazlauskas A., Meistas E., 1992, *Baltic Astronomy*, 1, 149
- Sunada K., Nakazato T., Ikeda N., Hongo S., Kitamura Y., Yang J., 2007, *PASJ*, 59, 1185
- Turner B. E., Pirogov L., Minh Y. C., 1997, *ApJ*, 483, 235
- van den Ancker M. E., de Winter D., Tjin A. Djie H. R. E., 1998, *A&A*, 330, 145
- Walsh A. J., Myers P. C., Burton M. G., 2004, *ApJ*, 614, 194
- Wang S., Looney L. W., Brandner W., Close L. M., 2008, *ApJ*, 673, 315
- Werner M. W., et al., 2004, *ApJS*, 154, 1
- Williams J. P., Bergin E. A., Caselli P., Myers P. C., Plume R., 1998, *ApJ*, 503, 689
- Wilson T. L., Rood R., 1994, *ARA&A*, 32, 191
- Wu J., Evans N. J., II, 2003, *ApJ*, 592, L79
- Wu Y., Henkel C., Xue R., Guan X., Miller M., 2007, *ApJ*, 669, L37
- Wu Y., Huang M., He J., 1996, *A&AS*, 115, 283
- Wu Y., Zhou S., Evans N. J., II, 1992, *ApJ*, 394, 196
- Wu Y., Zhu M., Wei Y., Xu D., Zhang Q., Fiege J. D., 2005, *ApJ*, 628, L57
- Zhou S., Evans N. J., II, Koempe C., Walmsley C. M., 1993, *ApJ*, 404, 232
- Zhou S., Wu Y., Evans N. J., II, Fuller G. A., Myers P. C., 1989, *ApJ*, 346, 168